Hindawi
Complexity
Volume 2020, Article ID 2917684, 13 pages
https://doi.org/10.1155/2020/2917684

Research Article

A Robust Control Strategy for Landing an Unmanned Aerial Vehicle on a Vertically Moving Platform

Carlos Aguilar-Ibanez,[1] **Miguel S. Suarez-Castanon**,[2] **Octavio Gutierrez-Frias**,[3] **Jose de Jesus Rubio**,[4] **and Jesus A. Meda-Campana**[4]

[1]*CIC, Instituto Politecnico Nacional, Av. Juan de Dios Batiz s/n, U.P.A.L.M, Ciudad de Mexico 07738, Mexico*
[2]*ESCOM, Instituto Politecnico Nacional, Av. Juan de Dios Batiz s/n, U.P.A.L.M, Ciudad de Mexico 07738, Mexico*
[3]*UPIITA, Instituto Politecnico Nacional, Av. Instituto Politecnico Nacional 2580, Ciudad de Mexico 07340, Mexico*
[4]*SEPI ESIME Azcapotzalco, Instituto Politecnico Nacional, Av. de las Granjas no. 682, Ciudad de Mexico 02250, Mexico*

Correspondence should be addressed to Miguel S. Suarez-Castanon; sasuarez@prodigy.net.mx

Received 28 January 2020; Accepted 23 June 2020; Published 15 July 2020

Academic Editor: Qingling Wang

In this work, we solve the uncertain unmanned aerial vehicle smooth landing problem over a moving platform, assuming that the aircraft position relative to the platform and its acceleration is always measurable. The landing task is carried out by an output-feedback robust controller, together with a repulsive force. The robust controller controls the nominal model, accomplishes the needed tracking trajectory, and counteracts the unknown uncertainties. To assure that the aircraft is always above the platform, we include a repulsive force that only works in a small vicinity of the platform. To estimate the relative aircraft velocity and platform acceleration, we use a supertwisting-based observer, assuring finite-time convergence of these signals. This fact allowed us to design the feedback state stabilizer independently of the observer design (in accordance with the separation principle). We confirmed the effectiveness of our control approach by convincing numerical simulations.

1. Introduction

The challenge of landing unmanned aerial vehicles on moving platforms has attracted the attention of several researchers in the control community. It is a problem that, if solved, has many applications, such as landing an unmanned aerial vehicle (UAV) on the deck of a ship in high seas. This control task consists of regulating to zero the relative distance between the aircraft and the ship deck, the latter being subject to external motions, including pitch or vertical movements. This regulation task has to be accomplished smoothly, safely, precisely, and fast, with the primary concern of safeguarding the physical integrity of both the aircraft and the ship. Usually, this control task has been accomplished using identification, adaptive algorithms, sliding-mode control, robust control, and optimal control [1–4]. In the literature, we can find several control schemes to address the UAV shipboard landing problem. In [2], an optical flow based control law for landing on a moving platform is proposed. In [5], a vision-based algorithm is presented, where the ground effect experienced during the maneuver task is compensated for using by a sliding adaptive control law. In [6], another vision-based landing algorithm for an autonomous helicopter is presented. The landing algorithm is integrated with algorithms for the visual acquisition of the target and navigation to the goal, from an arbitrary initial position and orientation. In [7], a control strategy for autonomously landing a helicopter on a rocking ship (due to rough seas) is presented. This control strategy is implemented by two controllers that separate the time scales of translation and rotation. Marconi et al. [1] present a control strategy for the autonomous landing of a vertical

take-off and landing vehicle (VTOL) on a ship with a deck that oscillates vertically due to high seas. There, the authors design an internal model-based error feedback dynamic regulator that is robust with respect to some uncertainties about the mechanical parameters that characterize the model and secures global convergence. Yang et al. [8] present a procedure for predicting a ship's pitch and heave motions. This procedure is based on a predictive controller whose inputs are measurements of relative distance and whose outputs are the predictions of the pitch movements. Other exciting works based on the predictive control approach to solving this control task are [9–12]. In [13], the UAV landing problem is addressed using a three-step procedure: motion estimation, trajectory generation, and tracking control, where the latter is accomplished as an optimal control. The optimal control approach for landing UAVs is also used in two recently published works [14, 15]. A full review of the literature related to this problem is beyond the scope of this work; however, we suggest to the interested reader the following works [16–25].

In this work, we approach the problems of feedback regulation and output regulation to accomplish the landing control maneuver task of successfully landing a vertical take-off and landing unmanned aerial vehicle (VTOL-UAV) over a vertically moving platform, under the assumptions that the vehicle model is partially known, and its relative position with respect to the platform and the VTOL-UAV vertical acceleration are both available. Due to the nature of this maneuver, we can formulate it as if it were a synchronization of two partially known systems, where the platform is the master, and the VTOL-UAV is the slave. To this end, we use the aircraft simplified dynamic model. That is, we neglected the dynamics of the other coordinates. That is, we assume that the aircraft horizontal and angular displacements are conveniently small, and in an actual implementation, such displacements can be eliminated by suitable robust controllers. Then, to solve this problem, we designed a control strategy were we first proposed a nonlinear control, consisting of two actions, in conjunction with a repulsive force. The first action, based on saturation, controls the nominal model, while the other action, which consists of a nonlinear integrator, compensates for the partially known nonlinearities. The controller and the compensator work together with the well-known supertwisting-based observer (STBO), which is in charge of estimates on a finite-time vehicle's relative velocity and moving platform's acceleration. The complementary repulsive force helps to guarantee that the aircraft is always above the platform. We use the Lyapunov method to carry out the closed-loop stability analysis. The novelty of this study is that, as far as we know, the Bézier spline-based trajectory planning in conjunction with a repulsive force has not been used before to solve the aforementioned control problem.

We organized the remainder of the study as follows: in Section 2, we introduce the VTOL-UAV model and establish the control problem; we develop the corresponding control strategy in Section 3, where we implement the needed STBO; in Section 4, we present the outcomes of the numerical simulations, which allow us to claim that our control strategy effectively lands the VTOL-UAV over the moving platform; finally, Section 5 gives the conclusions and final remarks.

Notation: the symbols $s_m[*]$ and $\operatorname{sgn}[x]$ refer, respectively, to a linear saturation function and the signum function of a real number, that is,

$$\begin{aligned} \operatorname{sgn}[x] &= \{1 \text{ if } x > 0; -1 \text{ if } x < 0; \in [-1,1] \text{ if } x = 0, \\ s_n[x] &= \{x \text{ if } |x| \le n \text{ else } n\operatorname{sgn}[x]. \end{aligned} \tag{1}$$

2. Problem Statement

To formally establish the control problem, we introduce a simplified model of a VTOL-UAV, described by the following system of equations:

$$m\ddot{z} = K_g(h)u - mg, \tag{2}$$

where z is the vertical aircraft position; u is the actual vertical rotor's thrust; $h = z - z_d$ is the relative distance between the VTOL-UAV position, z, and the position of the vertical moving platform, z_d; m is the VTOL-UAV mass; g is the gravity force; and $K(h)$ is a nonlinear function modeled as follows (see equation (31) in [2]):

$$K(h) = \frac{1}{1 - \left(D_0/h + l_0\right)^2}, \tag{3}$$

where the positive constants D_0 and l_0, with $l_0 > D_0$, can be identified from the physical. This nonlinear function is the thrust that the VTOL rotors generate. When the VTOL is approaching to the ground, the rotors will generate more thrust for a given power. This phenomenon is known as the ground effect [26]. These parameters are related to the aircraft physical dimensions [27]. The platform position is modeled as

$$z_d = \sum_{i=1}^{n} A_i \sin\left(\omega_i t + \zeta_i\right), \tag{4}$$

where A_i is the amplitude of the $i-$th component of the sinusoidal motion, ω_i is the frequency, and ζ_i is the phase. Loosely speaking, z_d models the platform vertical oscillatory movement due to the ocean waves. Having introduced the simplified VTOL-UAV system model, we present the primary concern of this work.

2.1. Control Problem. Consider the problem (2), with measurable outputs $h_1 = z - z_d$ and $y_2 = \ddot{z}$ and constants D_0 and l_0 unknown. The control objective consists in designing a control u such that

$$\begin{aligned} \left|z(t) - z_d(t)\right| &\le \delta_1, \\ \left|\dot{z}(t) - \dot{z}_d(t)\right| &\le \delta_2, \end{aligned} \tag{5}$$

for all $t > T > 0$ and where δ_1 and δ_2 are sufficiently small. In other words, we desire to render the system variables $(z(t), \ddot{z}(t))$ to a neighborhood of zero. That is to say, we want states $(z, \dot{z})$ of the VTOL-UAV to converge with that of

the platform $(z_d, \dot{z}_d)$, with sufficient accuracy for some $T > 0$, restricted to $z(t) \geq z_d(t)$ for all $t \geq 0$.

To solve the control problem mentioned above, we introduce the following assumptions:

A1: $|z_d^{(i)}(t)| \leq \overline{z}_i$, with $i = \{0, 1, 2\}$ and $t > 0$

A2: the signals $\ddot{z}(t)$ and $h(t)$ are always measurable

Notice that we must assure that $z(t) \geq z_d(t)$ for all $t \geq 0$ because we assume that the VTOL-UAV is always above the platform. This control problem resembles, for instance, the landing of a helicopter on a ship whose deck oscillates vertically due to sea waves, as depicted in Figure 1. We must note that the reference signal $z_d(t)$ and its first and second time derivatives have to be bounded (see $\overline{z}_i$, with $i = \{0, 1, 2\}$). On the contrary, we deal with the ideal case when signals h_1 and y_2 are noise free. However, if these signals are not noise free, we can overcome this problem filtering them using, for instance, a low-pass filter, obtaining the signals average values, which are very close to their actual values.

We finish this section by introducing a useful lemma, used in the forthcoming developments.

Lemma 1. *Consider the following uncertain second-order system:*

$$\begin{aligned} \dot{x} &= y; \\ \dot{y} &= v + \dot{\varphi}(t), \end{aligned} \tag{6}$$

where x, $y \in \mathbf{R}$ are the states, $\dot{\varphi}(t)$ is a continuous bounded perturbation, and v is the system input, defined as

$$v = -s_a[y - \dot{x}_r] - s_{a/2}[x + y - (x_r + \dot{x}_r)] + \ddot{x}_r, \tag{7}$$

where $a > 0$ is a constant and x_r is the smooth reference signal with time derivatives $\dot{x}_r$ and $\ddot{x}_r$. Suppose that $|x_r^{(i)}| \leq \overline{x}_r^{(i)}$ with $i = \{0, 1, 2\}$, $|\dot{\varphi}(t)| \leq \overline{\dot{\varphi}}$, and $\dot{\varphi}(t) \longrightarrow 0$, as long as $t \longrightarrow \infty$, with

$$\int_0^\infty |\varphi(t)| \mathrm{d}t \leq M < \infty, \tag{8}$$

then the tracking errors, $e_x = x - x_r$ and $e_y = y - \dot{x}_r$, globally and asymptotically converge to the origin. Notice that $\overline{x}_r^{(i)}$ with $i = \{0, 1, 2\}$ are strictly positive and constant bounds.

The proof of this lemma can be found in Appendix.

Remark 1. We must emphasize that the signal v (refST0) is a bounded control. Consequently, it can be substituted by any other bounded controller, like a nested saturation-based controller, or by a twisting controller. For instance, the twisting controller

$$v = -\frac{a}{2}\operatorname{sgn}[y - \dot{x}_r] - a\operatorname{sgn}[x - x_r] + \ddot{x}_r \tag{9}$$

can be a suitable candidate. However, we use (7) because its stability analysis is easy to carry out.

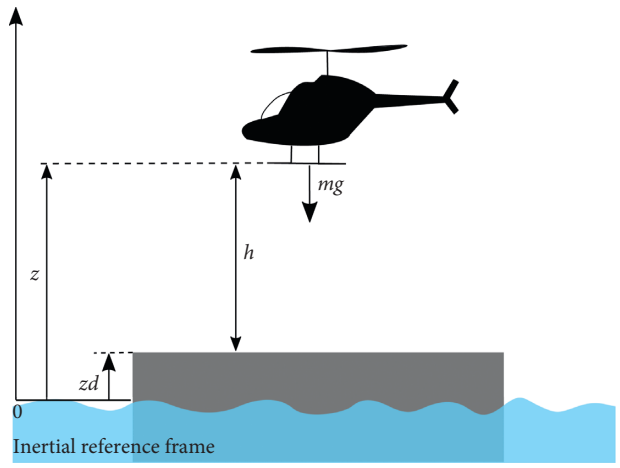

Figure 1: The VTOL-UAV landing task over a vertically moving platform.

3. Control Strategy

Roughly speaking, we can see the control problem established above as an uncertain system synchronization problem, where the platform acts as the master and the VTOL-UAV as the slave. To this end, we propose an output-feedback robust controller, together with a repulsive field-based force. The robust controller is devoted to assuring tracking error convergence to zero of the nominal model, and it simultaneously compensates for the unmodeled nonlinearities. The repulsive force acts if $h < 0.5\delta_1$, where $\delta_1 > 0$ is related to the constant defined buffer zone. As we only have measurements of the relative position h and the VTOL-UAV vertical acceleration $\ddot{y}$, we estimate the unknown variables $\dot{h}$ and $\ddot{z}_d$ by using an STBO [28], assuming that $K(h)$ is also partially known. Having obtained $\dot{h}$ and $\ddot{z}_d$, we proceed to design a robust output-feedback-based controller together with a trajectory planner. The planner allows us to render the aircraft to the buffer zone and lands it very smoothly on the platform. We accomplish the reference trajectory h_r using a fifth-grade Bézier spline, allowing us to plan the landing time.

Comment 1. In our opinion, the advantage of our proposal is that we give a robust control-based solution, which considers the dynamic variations in function $K(h)$ given in (3), based on saturation functions, together with a nonlinear integrator. This combination has the advantage of solving the problem in a precise manner when the external perturbations have slow variations. Contrary, for instance, to the adaptive and PI control approaches where we use an approximation to solve this kind of problem, we assume that the time derivative of $K(h)$ is equal to zero. On the contrary, if we compare our strategy with other well-known strategies, it has the drawback of having a slower time response, and the control gain parameters are difficult to tune adequately.

3.1. Reconstruction of the Unknown Variables. Defining the synchronization errors as $h_1 = z - z_d$ and $h_2 = \dot{z} - \dot{z}_d$, we have that

$$\begin{aligned} \dot{h}_1 &= h_2, \\ \dot{h}_2 &= y_2 - \ddot{z}_d, \end{aligned} \tag{10}$$

where $y_2 = \ddot{z}$ is in fact a measurable signal. Then, for estimating the missing variables h_2 and $\ddot{z}_d$, we use the following observer [28, 29]:

$$\begin{aligned} \dot{\widehat{h}}_1 &= \widehat{h}_2 + \beta\left|h_1 - \widehat{h}_1\right|^{1/2}\operatorname{sgn}\left[h_1 - \widehat{h}_1\right], \\ \dot{\widehat{h}}_2 &= y_2 + \alpha\operatorname{sgn}\left[h_1 - \widehat{h}_1\right], \\ \tau\dot{\widehat{w}} &= -\widehat{w} + \alpha\operatorname{sgn}\left[h_1 - \widehat{h}_1\right], \end{aligned} \tag{11}$$

where constants α and β must be selected, such that

$$\begin{aligned} &\alpha > \overline{z}_2, \\ &\beta > \frac{(1+\zeta)(\alpha + \overline{z}_2)}{(1-\zeta)}\sqrt{\frac{2}{(\alpha - \overline{z}_2)}}, \end{aligned} \tag{12}$$

for some $\zeta \in (0,1)$ and $0 < \tau \ll 1$. Defining the observation errors as $e_{o_1} = h_1 - \widehat{h}_1$ and $e_{o_2} = h_2 - \widehat{h}_2$, we obtain, from the first two equations of (10) and (11), the following equations:

$$\begin{aligned} \dot{e}_{o_1} &= e_{o_2} - \beta\left|e_{o_1}\right|^{1/2}\operatorname{sgn}\left[e_{o_1}\right], \\ \dot{e}_{o_2} &= -\ddot{z}_d - \alpha\operatorname{sgn}\left[e_{o_1}\right]. \end{aligned} \tag{13}$$

As constants α and β are selected according to (12), we can assure that e_{o_1} and e_{o_2} asymptotically converge to zero in a finite time (for details see Sections III and IV of [28]). On the contrary, if we fix the step size of the numeric integration method, ς, such that $0 < \varsigma < \tau \ll 1$, then we can assure that $\widehat{w} \longrightarrow -\ddot{z}_d$ in a finite time, as long as $\tau \longrightarrow 0$ [29]. That is, there exists $T_0 > 0$, such that $\widehat{h}_2(t) = \dot{h}(t)$ and $\widehat{w}(t) = -\ddot{z}_d(t)$, for all $t > T_0$.

The disadvantage of this sliding-mode observer is that we need to know, at least, an estimated value for the constant $\overline{z}_2$. However, we can overcome this inconvenience by selecting the constant α large enough. Similarly, to reconstruct $\ddot{z}_d$, we need to select τ and ς small enough, depending on the natural frequency of $\ddot{z}_d$.

3.2. Robust Control Law. Since we can recover variables $\dot{h}$ and $\ddot{z}_d$ in a finite time, we propose a suitably robust control scheme for assuring that h_1 and h_2 asymptotically converge to zero. Before proceeding, we introduce the following useful proposition.

Proposition 1. *Let us consider the following uncertain second-order system:*

$$\begin{aligned} \dot{q} &= p, \\ \dot{p} &= b(x,t)u + \phi(t), \end{aligned} \tag{14}$$

where q and $p \in R$ are the states, $x = [q,p]^T$, $u \in R$ is the system input, and $b(x,t)$ and $\phi(t) \in R$ are partially unknown functions. Let as assume the following:

P1: there exits $\underline{b} > 0$ and $\overline{b} > 0$, such that $\underline{b} \le b(x,t) \le \overline{b}$, for $t \ge 0$

P2: $|\phi(t)| \le \overline{\phi}(t) < \infty$ for all $t \ge 0$

Consider the following controller:

$$u = \frac{1}{\overline{b}}(v_d + \zeta), \tag{15}$$

$$v_d = -s_{a/2}\left(e_q + e_p\right) - s_a\left(e_p\right) + \ddot{q}_d, \tag{16}$$

where $e_q = q - q_d$, $e_p = p - \dot{q}_d$, and q_d is the continuous and bounded reference trajectory, with the first and the second time derivatives being also continuous and bounded, and the auxiliary control ζ is defined as

$$\zeta = -\lambda_0\xi - \frac{\lambda_1\xi\left(\|v_d\| + \overline{\phi}(t)\right)}{k\exp\left(-\lambda_2 t\right) + \|\xi\|}, \tag{17}$$

with

$$\xi(t) = p(t) - p(0) - \int_0^t v_d(s)\mathrm{d}s, \tag{18}$$

where the parameters $\{\lambda_0, \lambda_1, \lambda_2, k\}$ are strictly positive with $\lambda_1 \underline{b}/\overline{b} > 1$. Then, the closed-loop systems (14) and (15) assure that the tracking errors, e_q and e_p, asymptotically converge to zero.

Proof. From (14) and (15), we can write the closed-loop system as

$$\begin{aligned} \dot{q} &= p, \\ \dot{p} &= v_d + \left(\frac{b(x,t)}{\overline{b}} - 1\right)v_d + \frac{b(x,t)}{\overline{b}}\zeta + \phi(x,t). \end{aligned} \tag{19}$$

Now, from the definition of (18), it is easy to see that we can express the equation above in a short way as

$$\begin{aligned} \dot{q} &= p; \\ \dot{p} &= v_d + \dot{\xi}. \end{aligned} \tag{20}$$

Before continuing with the stability analysis of the above system, we first show that $\dot{\xi}$ converges to zero. To this end, we must note that the variable ξ, given in (18), can also be expressed as

$$\xi(t) = \int_0^t \left(\frac{b(x(s),s)}{\overline{b}}z(s) + \left(\frac{b(x(s),s)}{\overline{b}} - 1\right)v_d(s) + \phi(x(s),s)\right)\mathrm{d}s. \tag{21}$$

Indeed, it can be justified using the simple integration of the second equation of (19) and the definition (18). From assumption P3, we must emphasize that ξ can be computed online with equation (18). Having defined the new system representation (20), we proceed to show that the virtual controller z (17) makes variables ξ and $\dot{\xi}$ to asymptotically

converge to zero. To this end, we substitute (17) into the time derivative of ξ, given in equation (15), leading to

$$\dot{\xi} = -\lambda_0 b^+(t)\xi - \lambda_1 b^+(t)\xi\left(\frac{|v_d| + \overline{\phi}(t)}{k\exp(-\lambda_2 t) + |\xi|}\right) + \left(b^+(t) - 1\right)v_d + \phi(x,t), \tag{22}$$

where

$$b^+(t) = \frac{b(x,t)}{\overline{b}}. \tag{23}$$

Hence, to analyze the behavior of the auxiliary variable ξ, we use the Lyapunov function $V = \xi^2/2$, in which the time derivative around the trajectories of (22) can be upper bounded as

$$\dot{V} \leq -\frac{\lambda_0 \underline{b}}{\overline{b}}\xi^2 + \frac{\left(-\overline{\lambda}_1 + 1\right)\xi^2 W(t)}{k\exp(-\lambda_2 t) + |\xi|} + \frac{k\exp(-\lambda_2 t)|\xi| W(t)}{k\exp(-\lambda_2 t) + |\xi|}, \tag{24}$$

where $\overline{\lambda}_1 = \lambda_1 \underline{b}/\overline{b}$ and $W(t) = |v_d| + \overline{\phi}(t) \leq \overline{W}$. Hence, selecting $\overline{\lambda}_1 = \lambda_1 \underline{b}/\overline{b} > 1$ and using P1, we obtain that the following inequality

$$\dot{V} \leq -\frac{2\lambda_0 \underline{b}}{\overline{b}}V + k\overline{W}\exp(-\lambda_2 t) \tag{25}$$

holds. From the last differential inequality, it is easy to conclude that V exponentially converges to zero (see Appendix). Hence, the variable $|\xi|$ also exponentially converges to zero. Now, as v_d (16) and $\overline{\phi}(t)$ are bounded, then $\dot{\xi}$ is bounded (see (22)), implying that ξ is uniformly continuous with $\xi \longrightarrow 0$, as long as $t \longrightarrow \infty$. Thus, according to the lemma of Barbalat, we can conclude that $\dot{\xi} \longrightarrow 0$, as long as $t \longrightarrow \infty$.

Finally, after substituting (16) into equation (20), we obtain

$$\begin{aligned} \dot{e}_q &= e_p; \\ \dot{e}_p &= -s_{a/2}\left(e_q + e_p\right) - s_a\left(e_p\right) + \dot{\xi}, \end{aligned} \tag{26}$$

where $\dot{\xi}$ is bounded and converges to zero. Besides, as $|\xi|$ exponentially converges to zero, we have that $\int_0^\infty |\xi(s)|\mathrm{d}s \leq M < \infty$. Consequently, according to Lemma 1, we have that $(e_q, e_p) \longrightarrow 0$, as long as $t \longrightarrow \infty$.

Remark 2. If we substitute the auxiliary controller ζ, defined in (17), by

$$\zeta = -\lambda_0\xi - \lambda_1 \mathrm{sgn}[\xi]\left(\left\|v_d\right\| + \overline{\phi}(t)\right), \tag{27}$$

the variable ξ will converge in a finite time. On the contrary, the performance of system (14), in closed loop with (15) and (16), could be improved if we substituted controller v_d with any other control based on the saturation function, as follows:

$$v_d = -s_a\left(e_q + be_p\right) + \ddot{q}_d, \tag{28}$$

or

$$v_d = -s_a\left(e_p + s_a\left(e_q\right)\right) + \ddot{q}_d, \tag{29}$$

where a and b are both positive constants, conveniently tuned.

3.2.1. The Dynamical Synchronization Equation. Substituting the equation of the VTOL-UAV system (2) into equation (10), we obtain the following synchronization equation:

$$\begin{aligned} \dot{h}_1 &= h_2; \\ \dot{h}_2 &= K(h)u - \Phi(t), \end{aligned} \tag{30}$$

where $\Phi(t) = g - \ddot{z}_d(t)$ and $K(h) = K_g(h)/m$. Now, to propose the control u to assure $(h_1, h_2) \longrightarrow 0$, as long as $t \longrightarrow \infty$, we assume that we know $\underline{k}$, $\overline{k}$, and $\overline{\Phi}$ such that

$$|\Phi(t)| \leq \overline{\Phi}(t); \underline{k} \leq K(h) < \overline{k}. \tag{31}$$

To accomplish this, we introduce the main proposition of this work.

Proposition 2. *Consider system (30) in closed loop with*

$$u = \frac{1}{\underline{k}}\left(-s_{a/2}\left(h_1 + \widehat{h}_2 - h_r - \dot{h}_r\right) - s_a\left(\widehat{h}_2 - \dot{h}_r\right) + \ddot{h}_r + \zeta\right), \tag{32}$$

where h_r is a Bézier spline and $\widehat{h}_2$ and $\widehat{w}$ evolve according to the system equations in (11), restricted to (12), and ζ is proposed as

$$\zeta = -\lambda_0\xi - \frac{\lambda_1\xi\left(\left\|v_d\right\| + \overline{\Phi}\right)}{k\exp(-\lambda_2 t) + \|\xi\|}, \tag{33}$$

with

$$v_d = -s_{a/2}\left(h_1 + \widehat{h}_2 - h_r - \dot{h}_r\right) - s_a\left(\widehat{h}_2 - \dot{h}_r\right) + \ddot{h}_r, \tag{34}$$

$\overline{\Phi}(t) = |g + \widehat{w}|$, *and*

$$\xi(t) = \widehat{h}_2 - \int_0^t v_d(s)\mathrm{d}s. \tag{35}$$

If constants λ_1 and λ_2 satisfy $\lambda_1 \underline{k}/\overline{k} > 1$, then for any initial condition (h_1, h_2), we can assure that errors h_1 and h_2 asymptotically converge to zero.

Proof. See Appendix.

3.2.2. Planification of the Reference Trajectory h_r. To land the VTOL-UAV on the moving platform, we use a Bézier spline-based trajectory [30]. We most note that the Bézier spline allows us to design translation trajectories from one equilibrium point to another equilibrium point, in a previously fixed time. We propose this trajectory to bring the aircraft, from any initial condition $h_0 = h(t_0) > 0$, to the buffer zone $h_f = h(t_f) = \delta_1 > 0$ with δ_1 being sufficiently small and $t_f \gg t_0$ conveniently fixed. That is, we define $h_r(t)$ as

$$h_r(t) = h_0 + \rho\left(t, t_0, t_f\right)\left(h_f - h_0\right), \tag{36}$$

where $\rho(t, t_0, t_f)$ is the selected Bézier spline, which satisfies the following conditions:

$$\begin{aligned} \rho\left(t_0, t_0, t_f\right) &= 0, \\ \rho\left(t_f, t_0, t_f\right) &= 1, \end{aligned} \tag{37}$$

where a finite number of the time derivatives of $\rho(t, t_0, t_f)$ are set to zero at the initial and final maneuver times t_0 and t_f (for details, please refer [30]). To assure that both $h > 0$ for all times and that the controller u turns off when the VTOL-UAV reaches the buffer zone, we fixed it, for practical purpose, as

$$\Theta = \left\{\mathbf{h} = (h, \dot{h}) \colon \left(h^2 + 0.2\dot{h}^2\right)^{1/2} \leq 1.1\delta_1\right\}. \tag{38}$$

It is worthy to mention that Θ acts as decision function, which allows to decide when to deactivate the control action. That is, when the aircraft is above and close enough to the platform, the controller is set to zero; otherwise, it is on. Thus, we establish the practical control strategy as follows:

$$u = \frac{\mu}{\underline{k}}\left(v_d + u_r + \zeta\right), \tag{39}$$

where v_d and ζ are defined in Proposition 2 and μ is a function that acts as a switch and is defined as

$$\mu = \begin{cases} 0, & \text{if } \mathbf{h} \in \Theta, \\ 1, & \text{otherwise}, \end{cases} \tag{40}$$

and u_r is the repulsive force defined as

$$u_r = -\frac{\mathrm{d}}{\mathrm{d}h} U_{\mathrm{rep}}(h), \tag{41}$$

with its corresponding potential defined as

$$U_{\mathrm{rep}}(h) = \begin{cases} \dfrac{\delta_0^3}{2}\left(\dfrac{1}{h^2} - \dfrac{1}{\delta_0^2}\right)^2, & \text{if } h < \delta_0 \text{ and } \dot{h} < 0, \\ 0, & \text{otherwise}, \end{cases} \tag{42}$$

where $\delta_0 = 0.5\delta_1$. We must note that the repulsive force U_{rep} assures that $h \geq 0$. We omitted the stability proof of system (2) in closed loop with control (39) because it mimics Proposition 1.

Comment 2. Please note that the slower the aircraft descends, the lesser the possibility to crash it with the platform. We can expect the same result if we increase either the size of the buffer zone or the magnitude of the repulsive force, by conveniently tuning, for instance, δ_0 and t_f being sufficiently large. However, the crashing possibility cannot be avoided by any methodology, if an unexpected and strong enough crosswind appears suddenly.

4. Numerical Simulations

To assess the effectiveness of the proposed control strategy, we design and run three numerical experiments. In the first experiment, we perturb the aircraft with a crosswind. The second experiment consists of comparison among our control strategy (OCS), and the continuous and smooth PID-based strategy (PIDS), and an adaptive strategy (AS); the latter two are, respectively, proposed in [4, 13]. Finally, the third experiment is also a performance comparison, among OCS and a version of the discontinuous twisting-based strategy (TBS), found in [31].

4.1. Experiment Setup. We fix the system physical parameters as $m = 0.25\,\mathrm{kg}$, $D_0 = 1$, and $l_0 = 5$ and the controller gains, given in (15) to (17), as

$$\begin{aligned} \underline{k} &= 4, \\ \overline{k} &= 4.5, \\ a &= 3, \\ \lambda_0 &= 3, \\ \lambda_1 &= 2.2, \\ \lambda_2 &= 0.5, \end{aligned} \tag{43}$$

and the STBO gains as

$$\begin{aligned} \alpha &= 0.5, \\ \beta &= 3, \\ \tau &= 0.1. \end{aligned} \tag{44}$$

For the experiments two and three, we suppose that the system acceleration is noisily perturbed by a normally distributed random process with zero mean and whose standard deviation is 1, defined as

$$\Delta_s(t) = \frac{\eta(t)m}{5}, \tag{45}$$

where $\eta(t)$ is the random noise.

4.2. First Experiment. For this experiment, we fix the initial condition as $(h, \dot{h}) = (20.5, 0)$ and the Bézier spline parameters as $(t_0, t_f) = (0, 30)$ and simulate the platform hypothetical vertical movement, z_d, and the crosswind effect, Δ, as follows:

$$\begin{aligned} z_d(t) &= 0.25\sin\left(\frac{t}{2}\right)\cos\left(\frac{t}{2}\right); \\ \frac{\Delta(t)}{m} &= 0.2\sin^2\left(\frac{t}{4}\right) + 0.25. \end{aligned} \tag{46}$$

We show the outcome of this experiment in Figure 2, where we see that the VTOL-UAV reaches the buffer zone after 27 seconds and the estimated velocity matches the actual velocity after 5 seconds. Consequently, we can conclude that our control approach effectively lands the aircraft over the platform, with a good performance. In fact, the final error is in the order of 10^{-2} meters. We must note that there is a small error between h and h_r. This error can be explained because control v_d is based on a saturation function, which has the inconvenience of having a significant time of

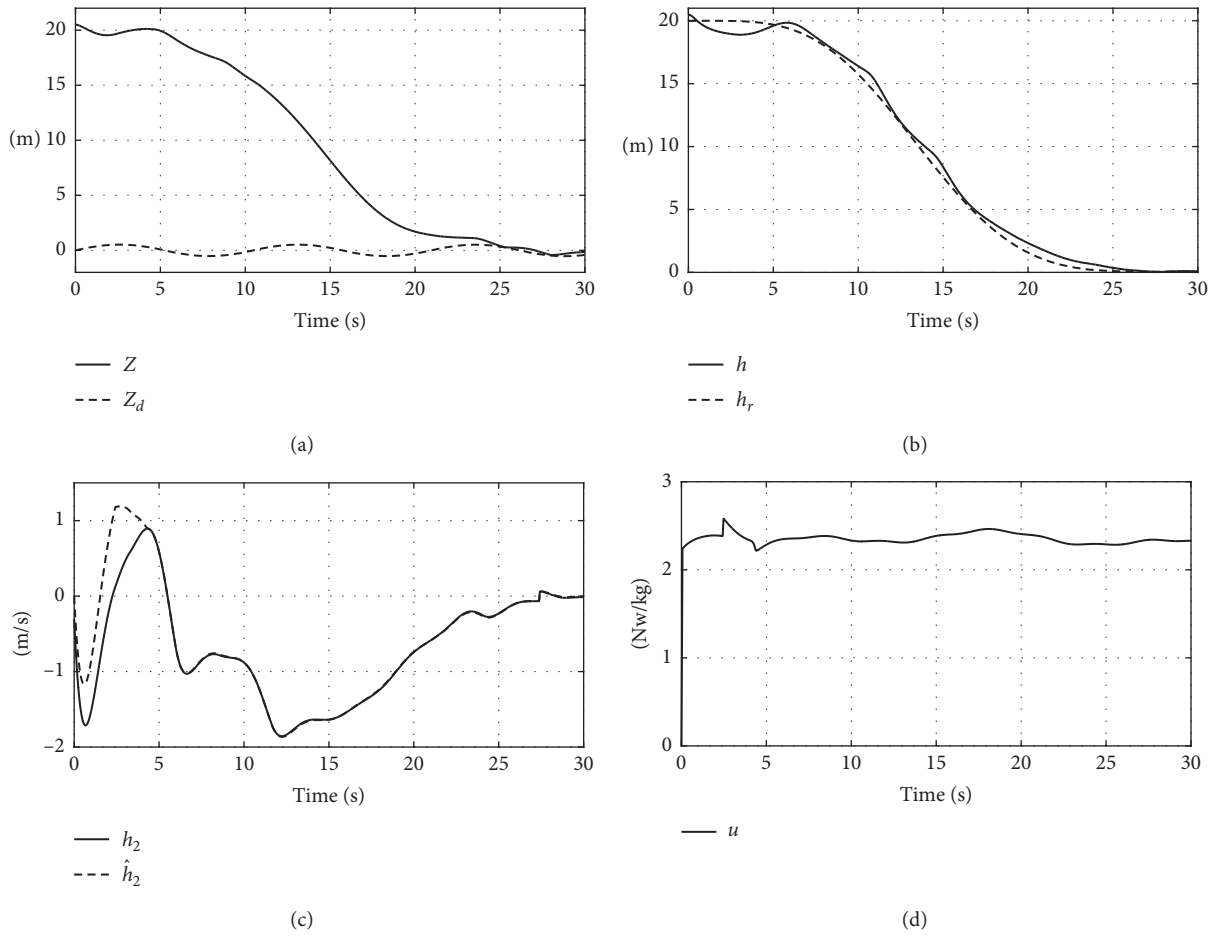

Figure 2: The closed-loop response of the VTOL-UAV perturbed by a crosswind when tracking a trajectory to land over a moving platform, with a programmed time of 30 seconds: (a) VTOL-UAV landing task; (b) comparison between actual and desired positions; (c) comparison between actual and desired velocities; (d) control action.

convergence. However, if time $t_f - t_0$ is sufficiently large, then we can improve the tracking error.

4.3. Second Experiment. For this experiment, we fix the initial condition as $(h, \dot{h}) = (10.5\,\text{m}.1\,\text{m/s})$ and the Bézier spline parameters as $(t_0, t_f) = (0, 30)$. We simulate the platform hypothetical vertical movement as in the first experiment, while we externally perturbed the system by a crosswind, defined as $\Delta(t)/m = 0.1\sin(t)\cos(t) + 0.1$, and we fixed the OCS saturation function parameter as $a = 6$. As we already mentioned, the experiment goal is to make a comparison among the OCS, PIDS, and AS strategies and to have an idea of how good our solution is with respect to the other two well-established approaches. In order to accomplish a fair comparison, we assume that $\dot{h}$ is measurable, and we add the repulsive force to the strategies PIDS and AS and use the same control gains for both strategies. Then, we propose the PIDS as

$$u = \frac{1}{\overline{b}}\left(-k_p\tilde{h}_1 - k_d\tilde{h}_2 - k_i\int_0^t \tilde{h}_1(s)\mathrm{d}s + \ddot{h}_r + 9.8 + u_r\right), \tag{47}$$

and the AS as

$$u = \widehat{d}\left(-k_p\tilde{h}_1 - k_d\tilde{h}_2 + \ddot{h}_r + 9.8 + u_r\right), \tag{48}$$

where $\overline{b} = 4$, $\tilde{h}_1 = h - h_r$, and $\tilde{h}_2 = \dot{h} - \dot{h}_r$ and $\widehat{d}$ is the gain parameter estimation of $K_g(h)$ based on the projective adaptive control law proposed in [13] and the control gains fixed as $k_p = 1$, $k_d = 2$, and $k_i = 1$, with u_r proposed as in (41). We show the obtained results from the numerical simulation in Figure 3. In this figure, we show the performance index of the three control strategies, which is defined as

$$I(T) = \frac{1}{T}\int_0^T\left(\tilde{h}_1^2(s) + \tilde{h}_2^2(s)\right)\mathrm{d}s, \tag{49}$$

and their corresponding control actions. From the performance indexes, we can see that OCS has a better performance than PIDS, while AS exhibits the less efficient performance index. In the same figure, we can see that the OCS control action shows fewer overshoots; however, the chattering phenomenon is always present. Between the PIDS and AS control actions, we can say that the first one exhibits more overshoots. We can also see that the PIDS strategy exhibits chattering when it is close to the equilibrium point, that is, after 20 seconds. Finally, in Figure 4 we show the trajectory tracking position error for the three control strategies. From this figure, we can

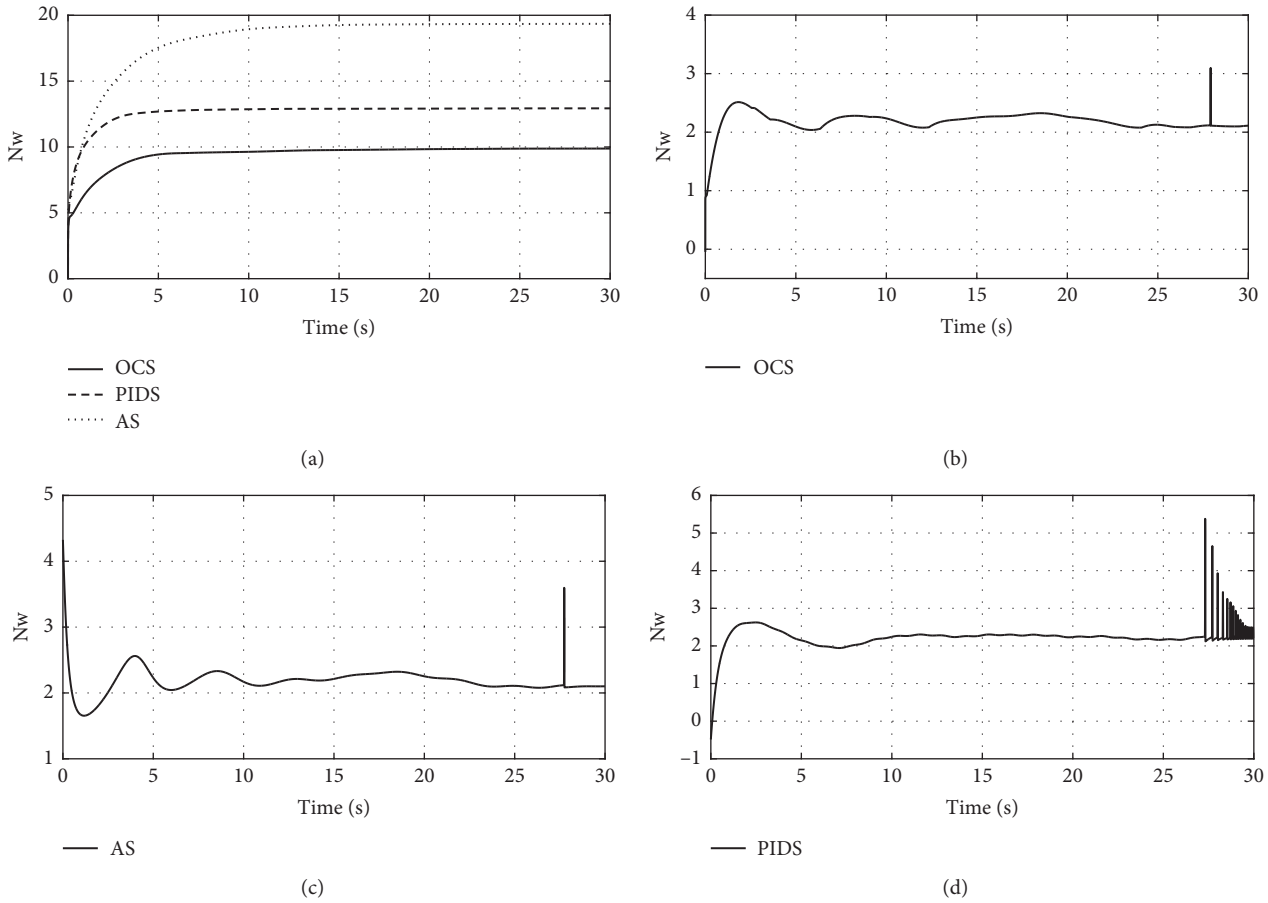

Figure 3: Comparison among the control strategies OCS, PID, and AS, when the system is perturbed by a normally distributed random process with zero mean.

see that OCS has a slightly better performance. Please note that the overshoots that we can see after 27 seconds are due to the effect of the repulsive force.

4.4. Third Experiment. The control task is the same as in the second experiment, but we fix the *Bézier* parameters as $(t_0, t_f) = (0, 50)$. In this experiment, once again, we perturbed the acceleration equation by adding it to the noisy signal $\Delta_s(t)$. Additionally, to make the experiment more realistic and illustrative, we added a noise signal to the output y. That is, $y_m = y_a + 0.1 \times \eta(t)$, where y_m and y_a are, respectively, the measurable and actual outputs, and $\eta(t)$ is a normally distributed random process with zero mean; we assume that $\dot{h}$ is not available and estimated using the STBO (11). Then, we use the following TBS:

$$u = -r_1 \operatorname{sign}\left[\tilde{h}_1\right] - r_2 \operatorname{sign}\left[\tilde{h}_2\right] + u_r, \tag{50}$$

where the controller gains satisfy $r_1 > r_2 > 0$ and the following conditions:

$$r_2 + \frac{C}{\underline{k}} < r_1 < \frac{(\bar{k} - \underline{k}) r_2 - 2C}{\bar{k} - \underline{k}}, \tag{51}$$

where

$$C = \max \overline{\Phi}(t) + c_i, \tag{52}$$

and $c_i > 0$ is any constant. We most note that, for this experiment, we fix $C = 5$. Hence, according to (51), we can select $r_1 = 10$ and $r_2 = 19$. Then, to make the comparison, we use the following error index:

$$h_M = \sqrt{\tilde{h}_1^2 + \tilde{h}_2^2}. \tag{53}$$

We show the comparison outcome in Figure 5, where we can see that, as we expected, the TBS outperforms OCS because the closed-loop response of the TBS is almost immune to external matching perturbation, having the inconvenience of exhibiting the chattering phenomena in the controller, as we can see it in Figure 5, preventing its actual implementation. In favor of OCS, we mention that the controller has a smooth response, which, in our opinion, is due to the integration action because it is averaging the noise effect over the system. This behavior can allow us to implement OCS for real applications.

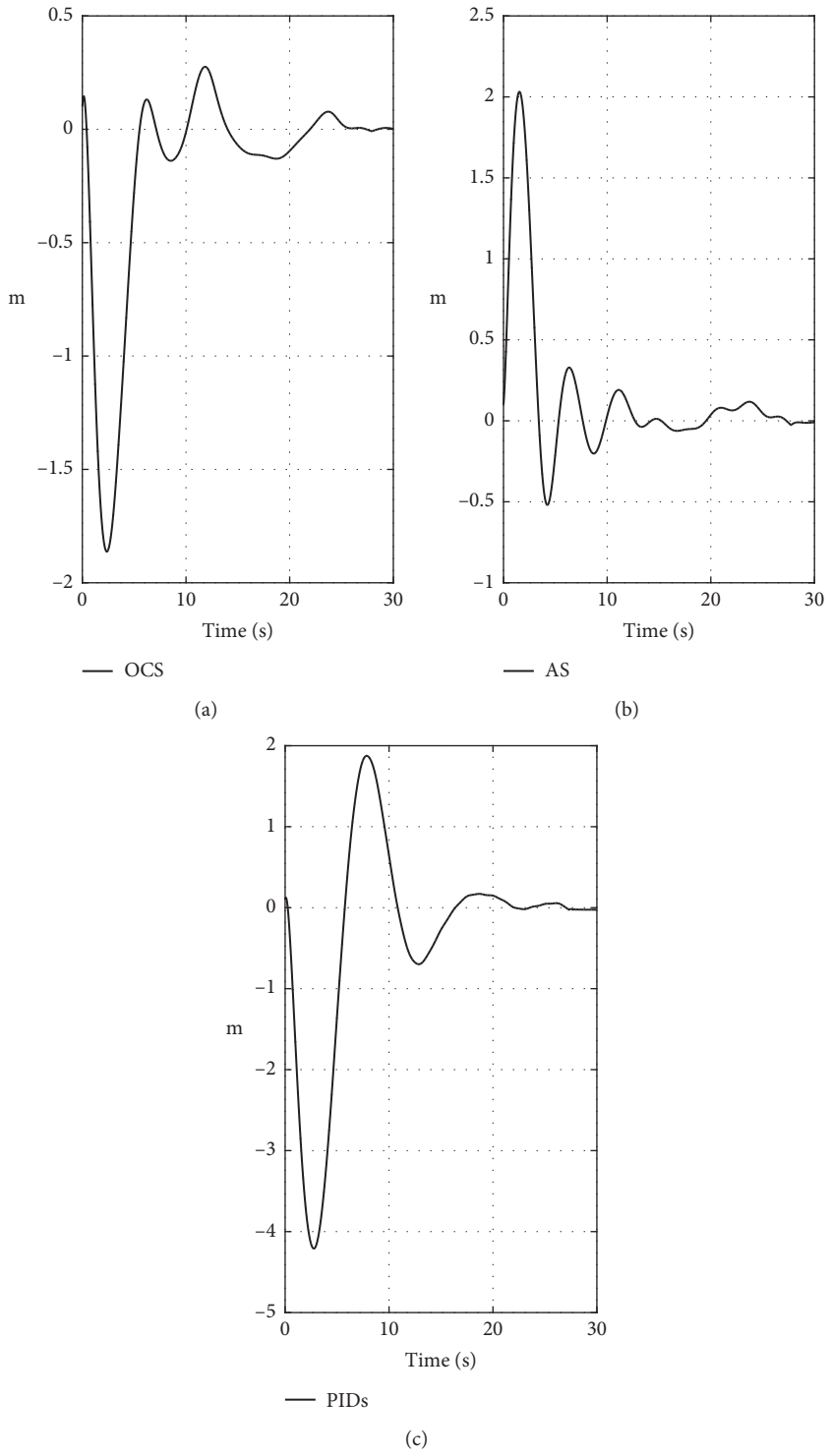

Figure 4: Comparison of the tracking trajectory position error $\widetilde{h} = h - h_r$ of strategies OCS, PID, and AS, when the system is perturbed by a crosswind.

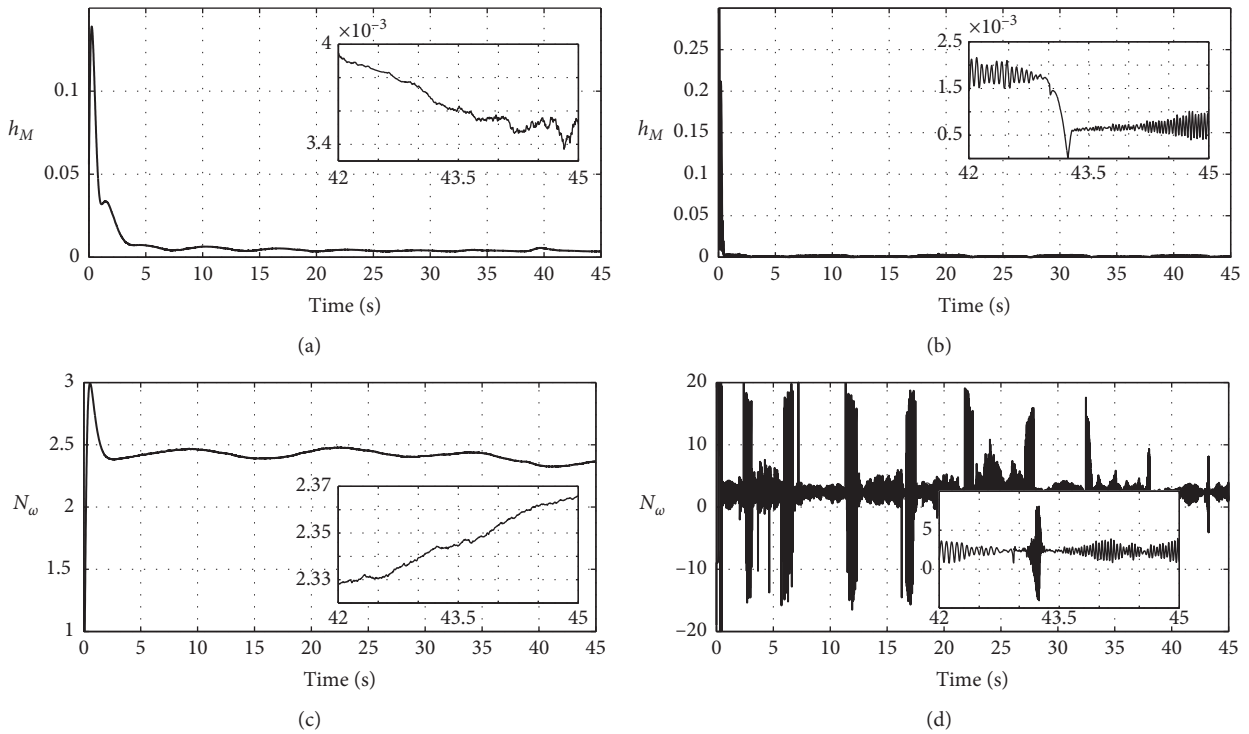

Figure 5: Comparison between the control strategies OCS and TBS, when the system is perturbed by a normally distributed random process with zero mean: (a) OCS error index; (b) TBS error index; (c) OCS control action; (d) TBS control action.

Comment 3. We must mention that we implement the sign function as

$$\operatorname{sign}(x) = \frac{x}{|x| + 10^{-3}}, \tag{54}$$

with integration step fixed as 10^{-4}.

5. Conclusions

In this work, we propose a control strategy for landing a VTOL-UAV smoothly on a vertically moving platform. We designed this control strategy assuming that the VTOL-UAV model was partially known, while its position relative to the platform and the platform acceleration were both available. Our landing control approach is based on designing an output-feedback robust controller, in conjunction with a repulsive force. The robust controller consists of two control actions: one based on saturation functions, and the other is a nonlinear integrator. The former controls the nominal model and assures the tracking trajectory task, and the latter compensates for the partially known uncertainties. Additionally, we introduce a repulsive force controller to guarantee that the aircraft is always above the platform, and it only works within a very small vicinity (buffer zone). We use an STBO to estimate the nonavailable aircraft relative velocity and the moving platform acceleration. We select the aircraft reference trajectory as a Bézier spline, devoted to bringing the system from any initial condition towards the buffer zone in a fixed time. To assess the effectiveness of our control method, we carry out two numerical simulations, the first of which performs the landing task when a crosswind perturbs the aircraft. The second experiment consists of a comparison among the strategies OCS and AS. From the results obtained in this simulation, shown in Figure 3, we can see that our control strategy has a better performance than the other two. Finally, we carry out the corresponding stability analysis based on the Lyapunov method.

Appendix

Proof. Proof of Inequality (25): first of all, multiplying both sides of (25) by $\exp(\bar{\lambda}t)$, we obtain

$$\frac{\mathrm{d}}{\mathrm{d}t}\left(V\exp(\bar{\lambda}t)\right) = \exp(\bar{\lambda}t)\left(\dot{V} + \bar{\lambda}V\right) \le k\overline{W}\exp\left(-\left(\lambda_2 - \bar{\lambda}\right)t\right), \tag{A.1}$$

where $\bar{\lambda} = 2\lambda_0\,\underline{b}/\bar{b}$. For simplicity, we suppose that $\lambda_2 \neq \bar{\lambda}$. Now, integrating both sides of the above inequality, we obtain

$$V\exp(\bar{\lambda}t) - V(0) \le k\overline{W}\left|\frac{1 - \exp\left(-\left(\lambda_2 - \bar{\lambda}\right)t\right)}{\lambda_2 - \bar{\lambda}}\right|, \tag{A.2}$$

which leads us, after using some simple algebra, to the following inequality:

$$V \le \exp(-\bar{\lambda}t)V(0) + \left|\frac{\exp(-\bar{\lambda}t) - \exp(-\lambda_2 t)}{\lambda_2 - \bar{\lambda}}\right|. \tag{A.3}$$

From the above, we conclude that V exponentially converges to zero. We can probe the case when $\lambda_2 = \bar{\lambda}$ is in a similar fashion.

Proof of Lemma 1: after some manipulation, it is easy to see that system (6), in closed loop with (7), can be written as

$$\begin{aligned}\dot{e}_x &= e_y,\\ \dot{e}_y &= -s_a\left[e_y\right] - s_{a/2}\left[e_x + e_y\right] + \dot{\varphi}(t),\end{aligned} \tag{A.4}$$

where $e_x = x - x_r$ and $e_y = y - \dot{x}_r$. Notice that the right-hand side of the equation above is Lipchitz, then states e_x and e_y remain bounded in a finite time. That is, the system is forward complete. Now, introducing the linear transformations $x_1 = e_x - e_y$ and $x_2 = e_y$ into system (A.4), we obtain

$$\begin{aligned}\dot{x}_1 &= x_2 - s_a\left[x_2\right] - s_{a/2}\left[x_1\right] + \dot{\varphi}(t),\\ \dot{x}_2 &= -s_a\left[x_2\right] - s_{a/2}\left[x_1\right] + \dot{\varphi}(t).\end{aligned} \tag{A.5}$$

Now, since $\dot{\varphi}(t) \longrightarrow 0$, as long as $t \longrightarrow \infty$, we can select $t_0 > 0$, such that $|\dot{\varphi}(t)| < a/4$, for all $t > t_0$. Thus, selecting the positive definite function $V_{(2)} = x_2^2/2$, we obtain that its time derivative, around the trajectories of the second equation of (A.5), leads to the following inequality:

$$\dot{V}_{(2)} \leq -x_2 s_a\left[x_2\right] + \frac{3a}{4}\left|x_2\right|. \tag{A.6}$$

Because system (A.5) is Lipchitz with respect to the states (x_1, x_2), they cannot exhibit finite time of escape. Notice that, if $|x_2| > a$, then from (A.6), we have that $\dot{V}_{(2)} < 0$. This implies that there exists $t_1 > t_0$, such that $|x_2(t)| < a$, for all $t > t_1$. When this condition is satisfied, we evidently have that $s_a[x_2] = x_2$. Consequently, the first equation of (A.5) reads as

$$\dot{x}_1 = -s_{a/2}\left[x_1\right] + \dot{\varphi}(t) \tag{A.7}$$

for all $t > t_1$. Using the positive definite function $V_{(1)} = x_1^2/2$ and recalling that $|\dot{\varphi}(t)| < a/4$, for all $t > t_1$, we have that the time derivative of $V_{(1)}$, around the trajectories of the system above, leads to the following inequality:

$$\dot{V}_{(1)} \leq -x_1 s_{a/2}\left[x_1\right] + \frac{a}{4}\left|x_1\right|. \tag{A.8}$$

Observe that, if $|x_1| > a/2$, then $\dot{V}_{(1)} < 0$. Thus, there exists a finite time $t_2 > t_1$ such that $|x_1(t)| \leq a/2$ for all $t \geq t_2$. After these conditions hold, system (A.5) reads as

$$\dot{x} = Ax + B\dot{\varphi}(t), \tag{A.9}$$

where $x = [x_1, x_2]^T$ and

$$\begin{aligned}A &= \begin{bmatrix} -1 & 0 \\ -1 & -1 \end{bmatrix},\\ B &= \begin{bmatrix} 1 \\ 1 \end{bmatrix}.\end{aligned} \tag{A.10}$$

According to (A.9), we have that

$$x(T) = e^{A\left(t - t_2\right)}x\left(t_2\right) + \int_{t_2}^{T} e^{A(t-s)}B\dot{\varphi}(s)\mathrm{d}s. \tag{A.11}$$

Using the integration by parts method into the equation above, we have that

$$\begin{aligned}x(T) = e^{A\left(t-t_2\right)}x\left(t_2\right) + B\varphi(T) - e^{At}B\varphi\left(t_2\right)\\ + \int_{t_2}^{T} e^{A(t-s)}B\varphi(s)\mathrm{d}s.\end{aligned} \tag{A.12}$$

Because the matrix A is Hurwitz, there exist $\alpha > 0$ and $\beta > 0$, such that

$$\left\|e^{At}\right\| \leq \beta e^{-\alpha t}. \tag{A.13}$$

Hence, the solution of (A.12) can be upper bounded as

$$\begin{aligned}\|x(T)\| \leq \beta_1 e^{-\alpha\left(T-t_2\right)} + \beta_0|\varphi(T)| + \beta_1 e^{-\alpha T}\left|\varphi\left(t_2\right)\right|\\ + \beta_2\int_{t_2}^{T} e^{-\alpha(T-s)}\|\varphi(s)\|\mathrm{d}s,\end{aligned} \tag{A.14}$$

where $\beta_0 = \|B\|$, $\beta_1 = \beta\|x(t_2)\|$, and $\beta_2 = \beta\|B\|$. Notice that

$$\begin{aligned}\int_{t_2}^{T} e^{-\alpha(T-s)}\|\varphi(s)\|\mathrm{d}s = \int_{t_2}^{T/2} e^{-\alpha(T-s)}\|\varphi(s)\|\mathrm{d}s\\ + \int_{T/2}^{T} e^{-\alpha(T-s)}\|\varphi(s)\|\mathrm{d}s.\end{aligned} \tag{A.15}$$

Now, using the Cauchy mean value theorem, we can upper bound the first term of the right-hand side of (A.15) as follows (the fact that $\int_0^\infty |\varphi(s)|\mathrm{d}s < M$ and $\dot{\varphi}(t)$ are bonded implies that $\varphi(t) \longrightarrow 0$, as long as, $t \longrightarrow \infty$):

$$\begin{aligned}\int_{t_2}^{T/2} e^{-\alpha(T-s)}|\varphi(s)|\mathrm{d}s = e^{-\alpha\left(T-t_*\right)}\int_{t_2}^{T/2}\|\varphi(s)\|\mathrm{d}s\\ \leq e^{-\alpha\left(T-t_*\right)}M,\end{aligned} \tag{A.16}$$

for some $t_* \in (t_2, T/2)$, leading us to conclude that

$$\lim_{T\longrightarrow\infty}\int_{t_2}^{T/2} e^{-\alpha(T-s)}|\varphi(s)|\mathrm{d}s = 0. \tag{A.17}$$

Similarly, the second term of the right-hand side of (A.15) satisfies the following equality:

$$\int_{T/2}^{T} e^{-\alpha(T-s)}\|\varphi(s)\|\mathrm{d}s = \left|\varphi\left(t^{**}\right)\right|\int_{t_2}^{T} e^{-\alpha(T-s)}\mathrm{d}s, \tag{A.18}$$

for some $t^{**} \in (T/2, T)$, implying that

$$\lim_{T\longrightarrow\infty}\int_{T/2}^{T} e^{-\alpha(T-s)}\|\varphi(s)\|\mathrm{d}s = 0. \tag{A.19}$$

Therefore, from inequalities (A.14)–(A.19), we conclude that the state x converges to zero for any initial condition. That is, system (A.4) converges globally and asymptotically to the origin.

Proof of Proposition 2. For simplicity, we carry out the proof assuming that $h_r = 0$. As $\widehat{h}_2$ and $\widehat{w}$ are estimated by the STBO (11), with its corresponding gains fulfilling condition (12), we can conclude that $(\widehat{h}_2, \widehat{w})$ converges in finite time to $(h_2, -\ddot{z}_d)$. That is,

$$\begin{aligned}\widehat{h}_2 &= h_2 + e_{o_2}(t),\\ \ddot{z}_d &= -\widehat{w} + \eta_w(t),\end{aligned} \tag{A.20}$$

with $\eta_h(t)$ and $\eta_w(t)$ bounded, such that $\eta_h(t) \longrightarrow 0$ and $\eta_w(t) \longrightarrow 0$, as long as $t \geq T_*$, with T_* being finite. Under these conditions, it is easy to see that the trajectories of the closed-loop system (32) with (30) does not escape to infinity for all $t \geq T_*$. Moreover, after $t \geq T_*$, signals u, v_d, $\xi(t)$, and $\overline{\Phi}(t)$ are given as follows:

$$\begin{aligned} u &= \frac{1}{\underline{k}}(v_d + \zeta), \\ v_d &= -s_{a/2}(h_1 + h_2) - s_a(h_2), \\ \xi(t) &= h_2 - \int_0^t v_d(s)\mathrm{d}s, \\ \overline{\Phi}(t) &= \left|g - \ddot{z}_d\right|, \end{aligned} \tag{A.21}$$

where z is defined in (33). As the above signals coincide with the expression given in Proposition 1, with $\lambda_1 \underline{k}/\overline{k} > 1$, then we can assure that h_1 and h_2 converge to zero, as long as $t \longrightarrow \infty$.

Data Availability

No data were used to support this study.

Conflicts of Interest

The authors declare that there are no conflicts of interest.

Acknowledgments

This research was supported by Secretaria de Investigacion y Posgrado of the Instituto Politecnico Nacional, under research grant nos. 20200671, 20201623, and 20201829.

References

[1] L. Marconi, A. Isidori, and A. Serrani, "Autonomous vertical landing on an oscillating platform: an internal-model based approach," *Automatica*, vol. 38, no. 1, pp. 21–32, 2002.

[2] B. Herissé, T. Hamel, R. Mahony, and F.-X. Russotto, "Landing a VTOL unmanned aerial vehicle on a moving platform using optical flow," *IEEE Transactions on Robotics*, vol. 28, no. 1, pp. 77–89, 2012.

[3] D. Mellinger, N. Michael, and V. Kumar, "Trajectory generation and control for precise aggressive maneuvers with quadrotors," *The International Journal of Robotics Research*, vol. 31, no. 5, pp. 664–674, 2012.

[4] B. Hu, Lu Lu, and S. Mishra, "Fast, safe and precise landing of a quadrotor on an oscillating platform," in *Proceedings of the American Control Conference (ACC)*, pp. 3836–3841, IEEE, Chicago, IL, USA, July 2015.

[5] D. Lee, T. Ryan, and H. J. Kim, "Autonomous landing of a VTOL UAV on a moving platform using image-based visual servoing," in *Proceedings of the 2012 IEEE International Conference on Robotics and Automation*, pp. 971–976, IEEE, Saint Paul, MN, USA, May 2012.

[6] S. Saripalli, J. F. Montgomery, and G. S. Sukhatme, "Visually guided landing of an unmanned aerial vehicle," *IEEE Transactions on Robotics and Automation*, vol. 19, no. 3, pp. 371–380, 2003.

[7] S.-R. Oh, K. Pathak, S. K. Agrawal, H. R. Pota, and M. Garratt, "Approaches for a tether-guided landing of an autonomous helicopter," *IEEE Transactions on Robotics*, vol. 22, no. 3, pp. 536–544, 2006.

[8] X. Yang, H. Pota, M. Garratt, and V. Ugrinovskii, "Prediction of vertical motions for landing operations of UAVS," in *Proceedings of the 2008 47th IEEE Conference on Decision and Control*, pp. 5048–5053, IEEE, Cancun, Mexico, December 2008.

[9] W. S. Ra and I. H. Whang, "Real-time long-term prediction of ship motion for fire control applications," *Electronics Letters*, vol. 42, no. 18, p. 1020, 2006.

[10] J. C. Chung, Z. Bien, and Y. S. Kim, "A note on ship-motion prediction based on wave-excitation input estimation," *IEEE Journal of Oceanic Engineering*, vol. 15, no. 3, pp. 244–250, 1990.

[11] M. Triantafyllou, M. Bodson, and M. Athans, "Real time estimation of ship motions using kalman filtering techniques," *IEEE Journal of Oceanic Engineering*, vol. 8, no. 1, pp. 9–20, 1983.

[12] X. Zhao, R. Xu, and C. Kwan, "Ship-motion prediction: algorithms and simulation results," in *Proceedings of the 2004 IEEE International Conference on Acoustics, Speech, and Signal Processing*, IEEE, Montreal, Canada, May 2004.

[13] B. Hu, L. Lu, and S. Mishra, "A control architecture for time-optimal landing of a quadrotor onto a moving platform," *Asian Journal of Control*, vol. 20, no. 5, pp. 1701–1712, 2017.

[14] K. Ling, D. Chow, A. Das, and S. L. Waslander, "Autonomous maritime landings for low-cost VTOL aerial vehicles," in *Proceedings of the 2014 Canadian Conference on Computer and Robot Vision*, pp. 32–39, IEEE, Montreal, Canada, May 2014.

[15] B. Hu and S. Mishra, "A time-optimal trajectory generation algorithm for quadrotor landing onto a moving platform," in *Proceedings of the American Control Conference (ACC)*, pp. 4183–4188, IEEE, Seattle, WA, USA, May 2017.

[16] J. W. Kim, Y. Jung, D. Lee, and D. H. Shim, "Outdoor autonomous landing on a moving platform for quadrotors using an omnidirectional camera," in *Proceedings of the 2014 International Conference on Unmanned Aircraft Systems (ICUAS)*, pp. 1243–1252, IEEE, Orlando, FL, USA, May 2014.

[17] J. Luis Sanchez-Lopez, J. Pestana, S. Saripalli, and P. Campoy, "An approach toward visual autonomous ship board landing of a VTOL UAV," *Journal of Intelligent & Robotic Systems*, vol. 74, no. 1-2, pp. 113–127, 2014.

[18] J. Luis Sanchez-Lopez, S. Saripalli, P. Campoy, J. Pestana, and C. Fu, "Toward visual autonomous ship board landing of a VTOL UAV," in *Proceedings of the 2013 International Conference on Unmanned Aircraft Systems (ICUAS)*, pp. 779–788, IEEE, Atlanta, GA, USA, May 2013.

[19] F. Ruffier and N. Franceschini, "Optic flow regulation in unsteady environments: a tethered MAV achieves terrain following and targeted landing over a moving platform," *Journal of Intelligent & Robotic Systems*, vol. 79, no. 2, pp. 275–293, 2015.

[20] J. Rubio Hervas, M. Reyhanoglu, and H. Tang, "Automatic landing control of unmanned aerial vehicles on moving platforms," in *Proceedings of the 2014 IEEE 23rd International Symposium on Industrial Electronics (ISIE)*, pp. 69–74, IEEE, Istanbul, Turkey, June 2014.

[21] J. Rubio Hervas, M. Reyhanoglu, and H. Tang, "Nonlinear automatic landing control of unmanned aerial vehicles on moving platforms via a 3D laser radar," *AIP Conference Proceedings*, vol. 1637, pp. 907–917, 2014.

[22] H. Liu, G. Lu, and Y. Zhong, "Robust output tracking control of a laboratory helicopter for automatic landing," *International Journal of Systems Science*, vol. 45, no. 11, pp. 2242–2250, 2014.

[23] L. R. G. Carrillo, E. Rondon, A. Sanchez, A. Dzul, and R. Lozano, "Stabilization and trajectory tracking of a quadrotor using vision," *Journal of Intelligent & Robotic Systems*, vol. 61, no. 1–4, pp. 103–118, 2011.

[24] A. Sanchez, P. Garcia, P. Castillo, and R. Lozano, "Simple real-time stabilization of vertical takeoff and landing aircraft with bounded signals," *Journal of Guidance, Control, and Dynamics*, vol. 31, no. 4, pp. 1166–1176, 2008.

[25] C. L. Castillo, W. Moreno, and K. P. Valavanis, "Unmanned helicopter waypoint trajectory tracking using model predictive control," in *Proceedings of the 2007 Mediterranean Conference on Control & Automation*, pp. 1–8, IEEE, Athens, Greece, June 2007.

[26] R. Mahony, V. Kumar, and P. Corke, "Multirotor aerial vehicles: Modeling, estimation, and control of quadrotor," *IEEE Robotics & Automation Magazine*, vol. 19, no. 3, pp. 20–32, 2012.

[27] P. Sanchez-Cuevas, G. Heredia, and A. Ollero, "Characterization of the aerodynamic ground effect and its influence in multirotor control," *International Journal of Aerospace Engineering*, vol. 2017, Article ID 1823056, 17 pages, 2017.

[28] J. Davila, L. Fridman, and A. Levant, "Second-order sliding-mode observer for mechanical systems," *IEEE Transactions on Automatic Control*, vol. 50, no. 11, pp. 1785–1789, 2005.

[29] J. Davila, L. Fridman, and A. Poznyak, "Observation and identification of mechanical systems via second order sliding modes," *International Journal of Control*, vol. 79, no. 10, pp. 1251–1262, 2006.

[30] H. Sira-Ramirez and S. K. Agrawal, *Differentially Flat Systems*, vol. 17, CRC Press, Boca Raton, FL, USA, 2004.

[31] A. Polyakov and A. Poznyak, "Unified lyapunov function for a finite-time stability analysis of relay second-order sliding mode control systems," *IMA Journal of Mathematical Control and Information*, vol. 29, no. 4, pp. 529–550, 2012.